PHYSICAL REVIEW B **91**, 214433 (2015)

Electronic structure, local magnetism, and spin-orbit effects of Ir(IV)-, Ir(V)-, and Ir(VI)-based compounds

M. A. Laguna-Marco,[1,2,*] P. Kayser,[2] J. A. Alonso,[2] M. J. Martínez-Lope,[2] M. van Veenendaal,[3,4] Y. Choi,[3] and D. Haskel[3]

[1]*Instituto de Ciencia de Materiales de Aragón and Departamento de Física de la Materia Condensada, CSIC–Universidad de Zaragoza, Zaragoza 50009, Spain*

[2]*Instituto de Ciencia de Materiales de Madrid, CSIC, Cantoblanco 28049 Madrid, Spain*

[3]*Advanced Photon Source, Argonne National Laboratory, Argonne, Illinois 60439, USA*

[4]*Department of Physics, Northern Illinois University, De Kalb, Illinois 60115, USA*

(Received 19 December 2014; revised manuscript received 30 April 2015; published 29 June 2015)

Element- and orbital-selective x-ray absorption and magnetic circular dichroism measurements are carried out to probe the electronic structure and magnetism of Ir 5*d* electronic states in double perovskite Sr_2MIrO_6 (M = Mg, Ca, Sc, Ti, Ni, Fe, Zn, In) and La_2NiIrO_6 compounds. All the studied systems present a significant influence of spin-orbit interactions in the electronic ground state. In addition, we find that the Ir 5*d* local magnetic moment shows different character depending on the oxidation state despite the net magnetization being similar for all the compounds. Ir carries an orbital contribution comparable to the spin contribution for Ir^{4+} ($5d^5$) and Ir^{5+} ($5d^4$) oxides, whereas the orbital contribution is quenched for Ir^{6+} ($5d^3$) samples. Incorporation of a magnetic 3*d* atom allows getting insight into the magnetic coupling between 5*d* and 3*d* transition metals. Together with previous susceptibility and neutron diffraction measurements, the results indicate that Ir carries a significant local magnetic moment even in samples without a 3*d* metal. The size of the (small) net magnetization of these compounds is a result of predominant antiferromagnetic interactions between local moments coupled with structural details of each perovskite structure.

DOI: 10.1103/PhysRevB.91.214433 PACS number(s): 78.70.Dm, 75.47.Lx, 75.70.Tj

I. INTRODUCTION

Transition-metal oxides with perovskite (or perovskite-related) structure are hosts to many fascinating phenomena: high-temperature superconductivity [1], colossal magnetoresistance [2,3], multiferroicity [4], metal-insulator transition [5–7], half-metallicity [8], etc. This abundance of behaviors has been further expanded with recent observations in iridium oxides, such as the localized-like transport and magnetism in Sr_2IrO_4 [9–11] and $BaIrO_3$ [12], the non-Fermi-liquid behavior in $SrIrO_3$ [13], and a spin-liquid ground state in $Na_4Ir_3O_8$ [14]. In addition, novel phases with unconventional electronic structures have been theoretically predicted: Mott insulators with orbital mediated exchange coupling in Kitaev-type models [15], layered quantum spin Hall systems [16], topological Mott insulators [17], spin liquids [18], axionic insulators and Weyl semimetals [19], and novel high-temperature superconductors [20]. Hypothetical double perovskite Sr_2CrIrO_6 should exhibit the highest T_C ever reported for half-metallic ferromagnets [21].

The strong spin-orbit coupling (SOC) in heavy 5*d* atoms is at the origin of this new wide variety of interesting electronic and magnetic properties. In these iridates, spin-orbit, crystal field, electronic bandwidth, Coulomb, and exchange interactions have comparable characteristic energy scales. This results in modification of the electronic band structure: the t_{2g} manifold created by the IrO_6 octahedral crystal electric field (CEF) is split (in the strong SOC limit) into reduced-bandwidth $J_{\text{eff}} = \frac{1}{2}, \frac{3}{2}$ bands. The half-filled, narrow $J_{\text{eff}} = \frac{1}{2}$ band can be further split via the relatively weak electron-electron interactions [9,10,15].

Recent works have shown that, as a result of these competing interactions, the ground state of the iridium oxides is highly tunable and the electronic structure and magnetic and transport properties are largely sensitive to changes in local environment, symmetry, or dimensionality [22–26]. As a result, these compounds become an interesting playground for the development of improved functional electronic and magnetic materials as the magnetic and transport properties can be tailored by slight alterations in the crystal structure driven by, for instance, chemical pressure introduced with elemental doping. A less explored route to modifying the electronic and magnetic properties is varying the occupation of the 5*d* band by control of Ir valence state.

The systematic study of double perovskites of the form $A_2BB'IrO_6$, with A = (Sr, La) and B, B' an alkaline earth metal or a d transition metal) is especially interesting. The ability of Ir to display different oxidation states (via doping and substitution at the A and B sites of the double-perovskite structure) may result in a rich variety of properties. Although Ir^{4+} is the most common oxidation state, Ir^{+3} has been found at the octahedral site of double perovskites such as Sr_2TaIrO_6 and Sr_2NbIrO_6 [27]. Ir^{5+} and Ir^{6+} can also be obtained under high oxygen pressure conditions. The stabilization of Ir^{5+} and Ir^{6+} is especially interesting because the Ir^{5+}-O and Ir^{6+}-O bonds should be among the strongest chemical bonds in an oxygen lattice, the degree of covalency expected to correlate with the magnetic-ordering temperatures.

We have undertaken a systematic x-ray diffraction (XRD), magnetic susceptibility, x-ray absorption near-edge structure (XANES) and x-ray magnetic circular dichroism (XMCD) study of double perovskites Sr_2MIrO_6 (M = Mg, Ca, Sc, Ti, Ni, Fe, Zn, In) and La_2NiIrO_6. By using different M atoms we are able to tune the oxidation state of Ir. Thus, we obtain Ir^{4+}, Ir^{5+}, and Ir^{6+} oxides, all with the same crystal structure.

*anlaguna@unizar.es

The XANES spectra allow us not only to check the oxidation state of iridium in each compound, but also to address the relevance of spin-orbit interactions. The XMCD measurements allow us to explore the dependence of the Ir orbital magnetic moment on the oxidation state. Since the orbital moment may have major effects on the magnetic anisotropy and coercivity, the disentanglement of the orbital contribution to the total magnetic moment is a key aspect of designing new functional magnetic materials. By studying oxides with nonmagnetic M atoms, we get a deeper understanding of the Ir $5d$ magnetism, namely, intrinsic versus induced, and whether the structural modifications driven by different M have significant effects on the magnetization (magnetic arrangement). Finally, with the introduction of a $3d$ magnetic cation in the B sublattice we explore the magnetic coupling between Ir and M ions, a key factor to finding novel materials with enhanced Curie temperatures.

II. EXPERIMENT

Polycrystalline samples of Sr_2MIrO_6 (M = Ca, Mg, Zn, In, Sc, Fe, Ni and Ti) and La_2NiIrO_6 were prepared via wet chemistry: the citrate-nitrate method. Subsequently, different annealing treatments were carried out between 900 °C–1100 °C to obtain the pure compounds. The oxides with Ir^{6+} oxidation state were prepared in an oxidizing atmosphere.

Structural characterization was done by means of powder x-ray diffraction (XRD) using a Bruker-AXS D8 diffractometer (40 kV, 30 mA), controlled by DRIFFACT^{PLUS} software, in Brag-Brentano reflection geometry with Cu $K\alpha$ radiation ($\lambda = 1.5418$ Å) and a PSD (Position Sensitive Detector). The diffraction patterns were Rietveld refined using the FULLPROF code [28]. The magnetic properties were studied with a commercial superconducting quantum interference device (SQUID) magnetometer from Quantum Design. The magnetic susceptibility was measured both in zero-field-cooled (ZFC) mode and field-cooled (FC) mode in the 4 K $\leqslant T \leqslant$ 400 K range under an applied magnetic field of 0.1 T. Isothermal magnetization curves were obtained for magnetic fields in the −5 to 5 T range at 4 K.

The XANES/XMCD measurements were carried out at beamline 4-ID-D of the Advanced Photon Source, Argonne National Laboratory. The spectra were recorded at the Ir $L_{2,3}$ absorption edges ($2p_{\frac{1}{2},\frac{3}{2}} \rightarrow 5d$ transition) to probe the Ir $5d$ states. Circularly polarized x rays were generated using phase-retarding optics [29,30]. XMCD was measured by switching x-ray helicity (12.7 Hz) and detecting the related modulation in absorption coefficient with a lock-in amplifier [31]. All the measurements were done in transmission geometry, at low temperature (5–8 K range) and under a magnetic field of 3.5 T applied along the x-ray propagation direction. For the measurement of the XAS and XMCD spectra, homogeneous layers of the powdered samples were made by spreading fine powders of the material onto an adhesive tape. Because of the very intense white line, the thickness and homogeneity of the samples were optimized to obtain a total absorption jump of ∼0.6 at about 70 eV above the L_3 edge, instead of the usual ∼1 jump. Harmonic rejection was achieved by the combined effects of x-ray reflection from two Pd mirrors at 3 mrad incidence angle and detuning of the second crystal in the Si(111) double-crystal monochromator.

III. RESULTS AND DISCUSSION

A. Structural characterization

Single phases of the double perovskites Sr_2MIrO_6 and La_2NiIrO_6 were obtained as black and well-crystallized powders. XRD patterns (Figs. 1 and 2) show sharp and well-defined peaks characteristic of perovskite-type structures. The compounds Sr_2MIrO_6 (M = Ca, Mg, Zn, Ni, Fe, Co, Sc and In) and La_2NiIrO_6 exhibit superstructure reflections (011) and (013) due to the rock-salt ordered arrangement of M and Ir cations in B and B' sites, combined with the tilting of the BO_6 octahedra. A detailed neutron powder diffraction (NPD) structural study can be found elsewhere [32–34]. For the ordered phases, the structure was described in a monoclinic unit cell, either $I2/m$ (No. 12) or $P2_1/n$ (No. 14) space groups, depending on the degree of structural distortion. On the other hand, the compound with M = Ti does not present an ordered structure, with one single position for Ir and Ti cations and crystallizing in the $Pbnm$ orthorhombic space group. The average Ir-O interatomic bond distance and its

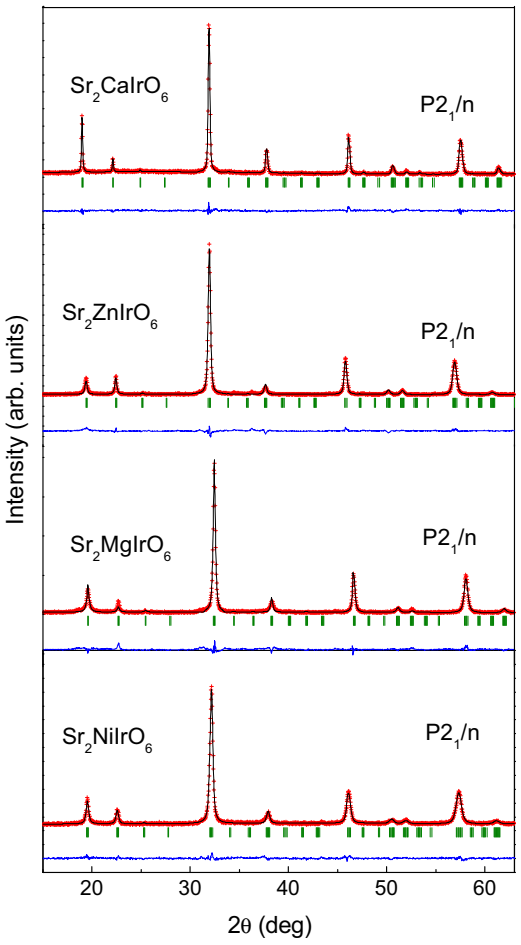

FIG. 1. (Color online) Observed (red symbol) calculated (black solid line) and difference (blue solid line) XRD Rietveld profiles for Sr_2MIrO_6 (M = Ca, Mg, Zn, Ni) at room temperature. Bragg reflections are marked with green bars.

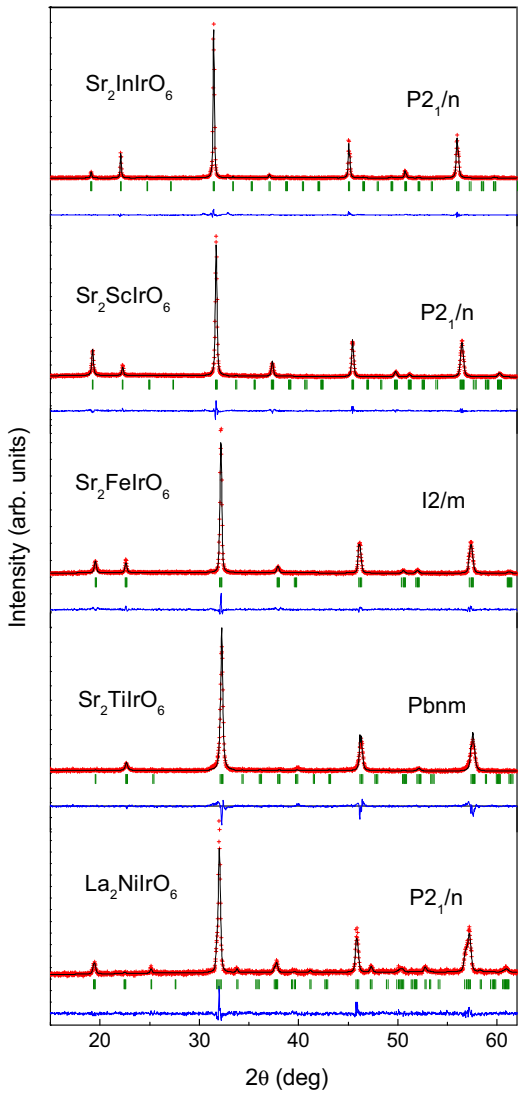

FIG. 2. (Color online) Observed (red symbol) calculated (black solid line) and difference (blue solid line) XRD Rietveld profiles for Sr_2MIrO_6 (M = Sc, In, Fe, Ti) and La_2NiIrO_6 at room temperature. Bragg reflections are marked with green bars.

deviation from octahedral geometry $\Delta(\text{Ir-O})_{\max}$, the average tilting of the M-O-Ir angle, and the degree of disorder in the M versus Ir occupancies at B, B' sites are listed in Table I. From the refined occupancy factors of oxygen atoms, a full stoichiometry is confirmed for all the compounds except for $Sr_2ZnIrO_{6-\delta}$ ($\delta = 0.13$) and $Sr_2MgIrO_{6-\delta}$ ($\delta = 0.11$).

B. Macroscopic magnetization

Figure 3 displays the magnetization versus magnetic field curves measured at 5 K for all the samples. The $M(H)$ curves of samples with M = Ca, Mg, and Zn present a linear response characteristic of antiferromagnetic (AFM) materials, whereas samples with Sc, In, or Ti present an S-shaped magnetization curve, which may be indicative of a major paramagnetic contribution. As for samples with magnetic M ions (bottom panel of Fig. 3), the Ni samples are collinear AFM, the net moment being due to canting induced by the external applied field. On the other hand, Sr_2FeIrO_6 is a weak ferromagnet with an intrinsic canting and showing a hysteresis loop.

TABLE I. Average Ir-O interatomic bond distance and its deviation from octahedral geometry (in Å), average tilting of the M-O-Ir angle (in degrees) and degree of disorder in the B (B') site determined from NPD at room temperature [32–34]. For those samples where the neutron scattering lengths between M and Ir are extremely similar to each other, the ordering was determined from XRD*.

Sample	Ir-O	$\Delta(\text{Ir-O})_{\max}$	ϕ	Occ.(M/Ir)
Sr_2MgIrO_6	1.957(14)	0.02	5.9	0.80(5)/0.20(5)
Sr_2CaIrO_6	1.939(3)	0.02	12.4	0.95(5)/0.05(2)
Sr_2ZnIrO_6	1.954(9)	0.02	7.8	0.87(3)/0.13(3)
Sr_2NiIrO_6	1.972(13)	0.04	6.8	0.92(2)/0.08(2)*
Sr_2ScIrO_6	1.99(1)	0.02	7.0	0.91(1)/0.09(1)*
Sr_2InIrO_6	1.99(1)	0.01	10.9	0.89(3)/0.11(3)
Sr_2FeIrO_6	1.96(2)	0.01	5.8	0.81(1)/0.18(1)*
Sr_2TiIrO_6	1.969(6)	0.01	5.8	No order
La_2NiIrO_6	2.028(9)	0.02	13.6	0.94(2)/0.06(2)

In contrast to the small net moment obtained at $T = 5$ K and $H = 3.5$ T, the effective magnetic moment obtained in the paramagnetic region indicates sizable local magnetic moments for Ir (in the 0.7–3.8 μ_B range, see Fig. 4). In addition, the negative values estimated for the Weiss temperature suggest

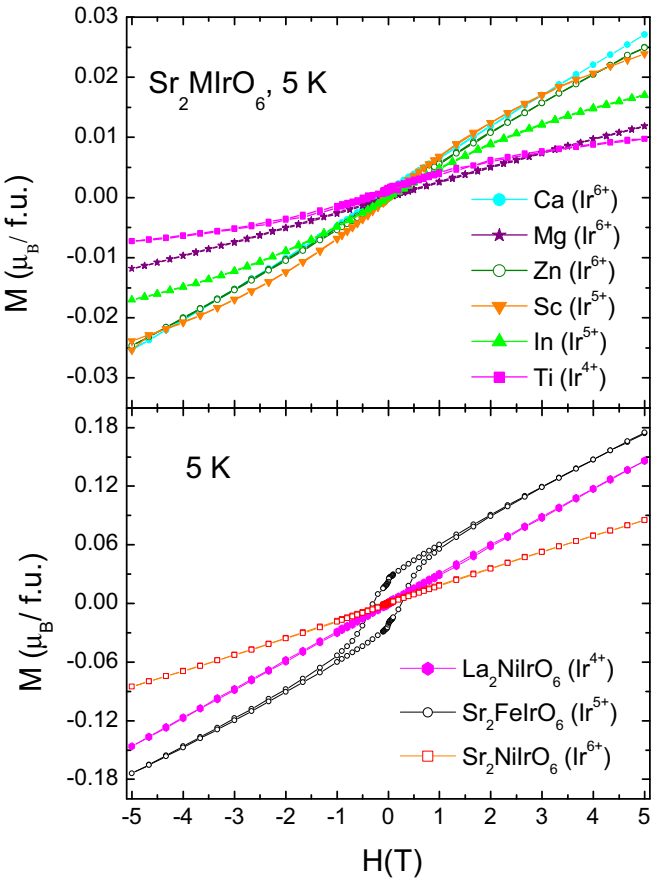

FIG. 3. (Color online) Magnetization vs applied field curves recorded at 5 K for compounds with nonmagnetic (top) and magnetic (bottom) M atom.

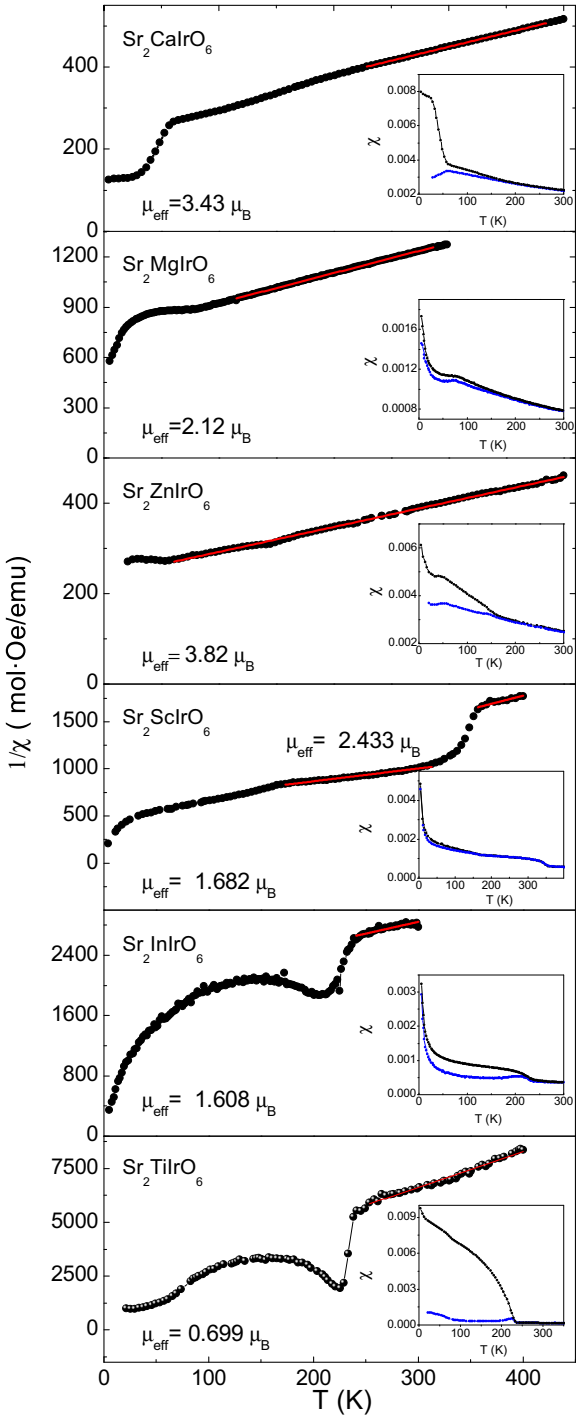

FIG. 4. (Color online) Reciprocal susceptibility vs temperature. The inset shows the thermal dependence of the field-cooled and zero-field-cooled dc magnetic susceptibility measured under 0.1 T.

that the main magnetic interactions are antiferromagnetic. This agrees with recent neutron diffraction measurements reporting a canted AFM arrangement of significant iridium magnetic moments on Sr_2CaIrO_6 [33]. Overall, the magnetization and susceptibility data indicate a complex scheme of magnetic interactions including competing antiferromagnetic interactions, paramagnetic contributions, and intersite disorder effects in these compounds.

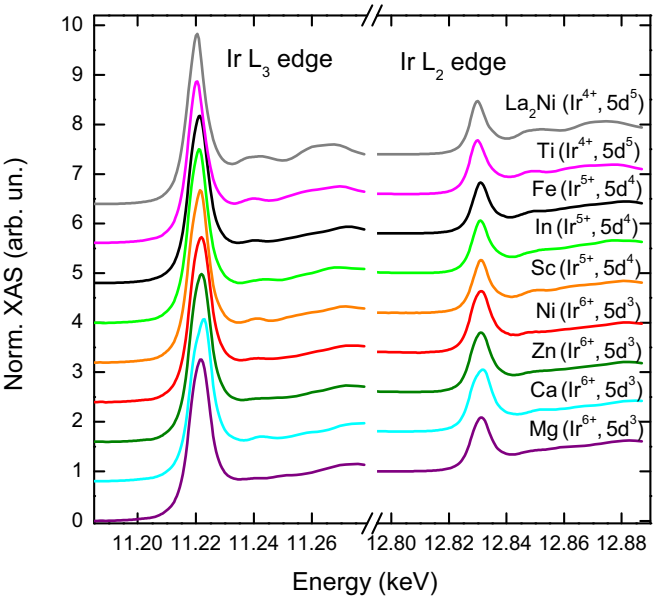

FIG. 5. (Color online) Ir $L_{3,2}$-edge XANES spectra recorded for a series of Ir-based oxides at $T = 6$ K. The spectra have been vertically shifted for the sake of clarity.

C. XANES and XMCD characterization

Figure 5 shows the Ir $L_{2,3}$-edge XANES spectra of the Sr_2MIrO_6, M = Mg, Ca, Sc, Ti, Ni, Fe, Zn, In, and La_2NiIrO_6 compounds at $T \sim 6$ K. All the samples show very intense "white lines" at both edges indicating a large local density of 5d states. Looking more in detail, however, clear differences can be observed in the XANES profiles indicating differences in the electronic structure among these compounds. In particular, three different groups of XANES spectra can be distinguished at the L_3 edge in relation to the electronic state of Ir in Fig. 6: the position of the L_3 white line shifts to higher energy in agreement with the expected electronic state: $5d^5$ (Ir^{4+}) for La_2NiIrO_6 and Sr_2TiIrO_6, $5d^4$ (Ir^{5+}) for M = Sc, Fe, and In, and $5d^3$ (Ir^{6+}) for Mg, Ca, Ni, and Zn samples. Smaller shifts can be also observed between compounds with the same nominal oxidation state of Ir. The energy shift of the absorption threshold is determined by the different Ir-O bond lengths (the shorter the interatomic distance, the higher the edge energy), which, in turn, gives a hint on the different oxidation state of the Ir ions [35–37]. Therefore, the energy shift can be used to get an estimation of the Ir valence for each compound. Using the energy position of Ca, Fe, and Ti as a reference and interpolating the rest of the samples to a linear dependence energy position versus valence, the resulting values are included in Table II. The XAS spectra indicate an Ir valence of 5.58+, 576+, and 5.82+ for Mg, Ni, and Zn, respectively, which might result in fractional or mixed valence in Ir. As for nominal Ir^{4+} and Ir^{5+} samples a 10% deviation from the nominal valence should not be ruled out. These results can be compared to estimates from neutron diffraction data, which indicate nominal valences hold for all compounds except Mg, Zn, and Ni. The presence of oxygen vacancies could explain the $Ir^{5.78+}$ and $Ir^{5.74+}$ states for Mg and Zn, respectively (∼4% deviation from the

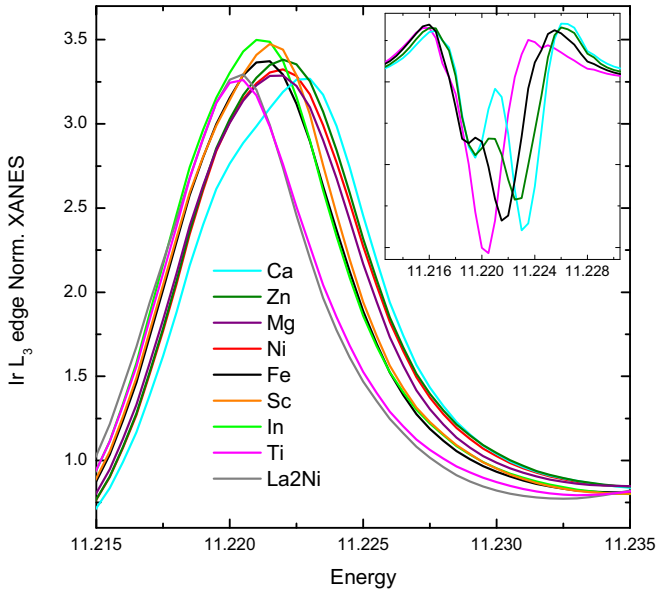

FIG. 6. (Color online) Detail of the XAS white line recorded at the Ir L_3 edge for a series of Ir-based oxides at $T = 6$ K. The inset shows the second derivative of four representative samples: Ti (Ir^{4+}), Fe (Ir^{5+}), Zn (Ir^{6+}), and Ca (Ir^{6+}).

nominal value). In the case of Ni the analysis of the Ir-O bond distances from ND suggest a $Ir^{5.15+}$ state [32–34]. In addition, we note that the occupation of the $5d$ orbitals may deviate from the nominal, integral valence occupation due to hybridization and band effects. For example, band-structure calculations yield $n_h = 5.37$ for the number of holes in the related compound Sr_2CoIrO_6, an 11% deviation from the nominal $5d^4$ configuration of Ir^{5+} states [38].

The L_3 white line feature gets broader as the oxidation state increases and the change in the integrated area provides another indicator of d-orbital occupancy variation in accordance with the observed energy shift. In addition, the spectral shape of samples with nominal Ir^{5+} and Ir^{6+} states shows an unresolved double-feature structure including a shoulder on the low-energy side of the peak. This subtle bimodal structure can be more clearly discerned in the profile of the second derivative of the spectra, as illustrated in the inset of Fig. 6. By comparison, in Ir^{4+} oxides no shoulder can be discerned at the white line and the second derivative only shows a very small shoulder at low energy. From the second derivative of the XANES spectra, the crystal field splitting has been obtained as the distance between the two peaks (see Table II).

At the L_2 edge, the threshold does not move towards higher energies as the oxidation state increases. More specifically, whereas Ir^{5+} and Ir^{4+} oxides follow the expected trend, the Ir^{6+} oxides have a very broad white line enveloping the former two white lines. Moreover, contrary to the L_3 case, the intensity of the L_2 white line is significantly larger (∼14%) for Ir^{6+} than for Ir^{5+} and Ir^{4+} oxides. In addition, it can be observed that the double-peak structure of the second derivative has disappeared at the L_2 edge for for $Ir^{4+}$and for Ir^{5+} samples.

For all the compounds, the branching ratio (i.e., the ratio of the integrated white line intensity recorded at the Ir $L_{2,3}$ edges, $\mathrm{BR} = I_{L_3}/I_{L_2}$) is clearly larger than the statistical BR of 2, characteristic of Ir metallic systems [39–42] (see Table II). In addition, the ground-state expectation value of the angular part of the spin-orbit coupling $\langle \mathbf{L}\cdot\mathbf{S}\rangle$, calculated via $\mathrm{BR} = (2 + \langle \mathbf{L}\cdot\mathbf{S}\rangle/n_h)/(1 - \langle \mathbf{L}\cdot\mathbf{S}\rangle/n_h)$ [43], ranges from ∼1.9 in Sr_2CaIrO_6 to ∼2.8 in Sr_2MIrO_6 (M = Sc, Fe, and In). This indicates a strong coupling between the local orbital and spin moments for all the compounds. Moreover, the high values of $\langle \mathbf{L}\cdot\mathbf{S}\rangle$ listed in Table II indicate a j_{eff}-like electronic ground state for all the compounds rather than an unsplit t_{2g}^n configuration (i.e., a ${}^{2S+1}T_{2g}$ state in octahedral symmetry with no spin-orbit coupling). Thus, in a pure j_{eff} picture with a spin-orbit coupling parameter of $\zeta \sim 0.3$ eV and a CEF splitting $10Dq \sim 3$ eV, the $\langle \mathbf{L}\cdot\mathbf{S}\rangle$ expected from configuration interaction calculations is ∼2.2, 3.4, and 2.4 for Ir^{4+}, Ir^{5+}, and Ir^{6+}, respectively [44]. That is, the $\langle \mathbf{L}\cdot\mathbf{S}\rangle$ goes up from Ir^{4+} to Ir^{5+} and then it goes back down again for Ir^{6+}, which is what can be seen Table II. The j_{eff}-like subband picture is further supported by the observed *anomalous* evolution of the L_2-edge white line with electron occupancy (Fig. 7). The strong enhancement for Ir^{6+} cannot be explained on the grounds of a $t_{2g} + e_g$ subband scheme, where both t_{2g} and e_g can be equally reached by the $p_{1/2}$ electrons, but it can be addressed to a j biased occupation driven by SOC where the empty states in Ir^{4+} ($5d^5$) and Ir^{5+} ($5d^4$) are mainly of $d_{5/2}$

TABLE II. Summary of results obtained from XAS and XMCD measurements: nominal valence, number of d holes n_h and electronic state of Ir, valence estimated from XAS shift, branching ratio, spin-orbit expectation value $\langle \mathbf{L}\cdot\mathbf{S}\rangle$ in units of $\hbar^2$, CEF in eV, Ir orbital, spin, and total magnetic moments given in μ_B/Ir. The spin magnetic moment has been calculated using $\langle T_z\rangle/\langle S_z\rangle$ obtained from numerical calculations: −0.087 for Ir^{4+}, 0.056 for Ir^{5+}, and 0.069 for Ir^{6+}.

Sample	Valence	n_h	$5d^x$	XAS valence (±0.22)	BR	$\langle \mathbf{L}\cdot\mathbf{S}\rangle$	CEF	m_l	m_s	m_s ($\langle Tz\rangle = 0$)	m_{tot}	L_z/S_z
Sr_2MgIrO_6	6+	7	$5d^3$	5.56+	3.78	2.60	3.0	0.000	0.013	0.016	0.013	0.00
Sr_2CaIrO_6	6+	7	$5d^3$	6.00+	3.08	1.85	3.8	0.000	0.023	0.028	0.022	−0.03
Sr_2ZnIrO_6	6+	7	$5d^3$	5.82+	3.56	2.39	3.1	0.001	0.020	0.025	0.021	0.05
Sr_2NiIrO_6	6+	7	$5d^3$	5.75+	3.25	2.07	3.0	−0.006	0.061	0.076	0.055	−0.19
Sr_2ScIrO_6	5+	6	$5d^4$	5.11+	4.58	2.78	3.2	0.003	0.005	0.006	0.008	1.01
Sr_2InIrO_6	5+	6	$5d^4$	4.95+	4.74	2.86	2.8	0.003	0.004	0.005	0.008	1.60
Sr_2FeIrO_6	5+	6	$5d^4$	5.00+	4.72	2.72	2.7	0.001	0.005	0.006	0.006	0.52
Sr_2TiIrO_6	4+	5	$5d^5$	4.00+	4.04	2.02	3.0	0.008	0.016	0.011	0.023	1.03
La_2NiIrO_6	4+	5	$5d^5$	3.86+	4.31	2.17	3.1	−0.017	−0.027	−0.018	−0.043	1.26

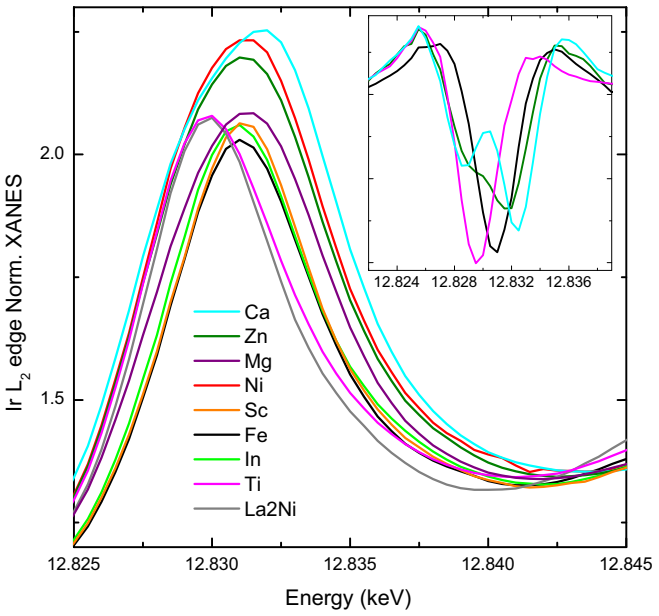

FIG. 7. (Color online) Detail of the XAS white line recorded at the Ir L_2 edge for a series of Ir-based oxides at $T = 6$ K. The inset shows the second derivative of four representative samples: Ti (Ir^{4+}), Fe (Ir^{5+}), Zn (Ir^{6+}), and Ca (Ir^{6+}).

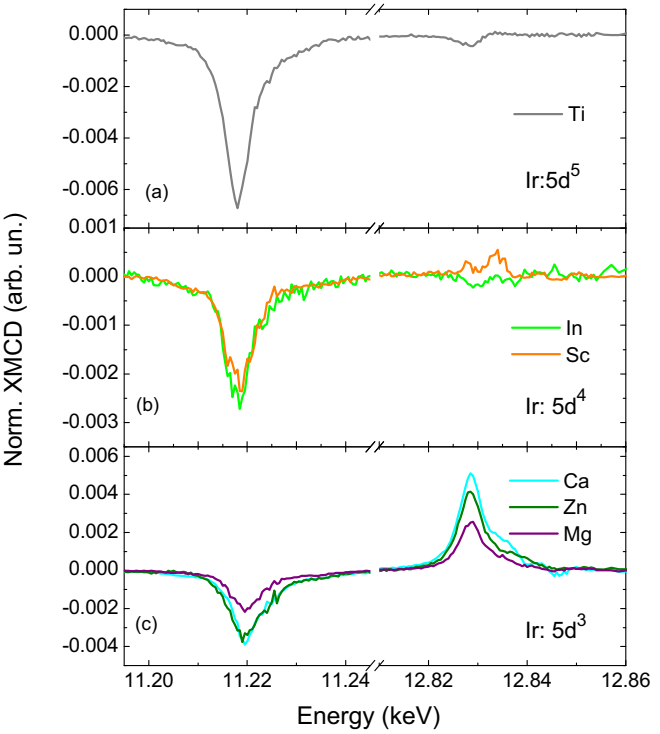

FIG. 8. (Color online) (a) Ir $L_{3,2}$-edge XMCD spectra of the Ir^{4+} oxides recorded at $T = 6$ K and $H = 3.5$ T. (b) Ir $L_{3,2}$-edge XMCD spectra of the Ir^{5+} oxides recorded at $T = 6$ K and $H = 3.5$ T. (c) Ir $L_{3,2}$-edge XMCD spectra of the Ir^{6+} oxides recorded at $T = 6$ K and $H = 3.5$ T.

character, whereas an additional orbital of $d_{3/2}$ character is empty in Ir^{6+} ($5d^3$).

Regarding the differences observed between the Ir^{6+} compounds, the small value of $\langle \mathbf{L} \cdot \mathbf{S} \rangle$ observed in Ca can be accounted for by its stronger CEF. On the other hand, the anomalous value found for Mg cannot be explained in terms of smaller CEF. Distortions from regular octahedral environment have been reported to play a role in the BR [23]. However, in this case diffraction refinements indicate similar distortions for all the compounds. The slightly smaller I-O-M tilting or the higher level of M/Ir antisite disorder may induce additional mixing. However, no clear relationship can be established at this point. In a similar way, no direct relationship can be established between $\langle \mathbf{L} \cdot \mathbf{S} \rangle$ and the fractional (or mixed) occupation of the $5d$ orbital derived from XAS or neutron diffraction (ND) (see Table II). In this respect, it is worth to note that the concomitant effect on $\langle \mathbf{L} \cdot \mathbf{S} \rangle$ is within the typical limits of the experimental uncertainties. For instance, a 5.75+ valence results in a 4% difference in $\langle \mathbf{L} \cdot \mathbf{S} \rangle$.

The XMCD corresponding to compounds without magnetic $3d$ atoms is shown in Fig. 8. Three different profiles can be distinguished correlated to the three different nominal electronic states of Ir. Ir^{6+} ($5d^3$) samples show signals of similar intensity at both edges and opposite sign. Besides, the intensity ratio is the same for the three compounds $L_2/L_3 \sim -1.24$. Very differently, for the Ir^{4+} ($5d^5$) sample the sign of the signal at both edges is the same. In addition, the amplitude of the XMCD at L_3 edge is much more intense than that at the L_2 edge (a factor of 15 for Sr_2TiIrO_6). In the Ir^{5+} ($5d^4$) compounds, the L_2-edge XMCD spectra are also clearly smaller than at the L_3 edge, but in this case the sign changes from one sample to another: it is opposite to the L_3 edge for Sc, but it has the same sign for In. Besides, overall, the intensity of the Ir^{5+} spectra is smaller than that of Ir^{4+} and Ir^{6+} compounds, e.g., at the L_3 edge the intensity of Sr_2InIrO_6 is 2.6 times smaller than that of Ti.

Sum-rules analysis indicates that the total magnetic moment ranges from ~0.006 up to 0.02 μ_B. These values are roughly in agreement with macroscopic magnetization measurements and with the XMCD-derived values reported for other Ir oxides [23,44]. The lack of a $3d$ magnetic moment in these samples demonstrates that the magnetic moment of Ir is intrinsic. Any magnetic moment imbalance is not induced by hybridization (polarization) with a magnetic $3d$ atom. On the other hand, since the normalized XMCD signal is proportional to the net (ordered) and not to the local (atomic) magnetic moment of Ir, the differences in m_{tot} between the samples cannot be directly related to a distinct atomic moment itself but might be due to the weakening of magnetic interactions (paramagnetic state) or variations in the degree of antiferromagnetic canting.

The m_l/m_s ratio, on the other hand, is a property of the atomic moment itself and the application of sum rules [45,46] reveals that the character of the magnetic moment (spin versus orbit) is strongly dependent on the oxidation state as shown in Table II. The samples with Ir^{4+} and Ir^{5+} have a significant orbital magnetic moment (m_l/m_s ~0.5, 0.8, and 0.5 for Sc, In, and Ti, respectively) that is parallel to the spin moment. On the other hand, in the case of Ir^{6+} samples (M = Mg, Ca, and Zn), the L_z/S_z ratio indicates a completely different character of the magnetic moment: the spin is much larger

than the orbital moment, which is almost quenched. In order to obtain $\langle S_z \rangle$ from sum rules, the $\langle T_z \rangle$ contribution has been determined by configuration interaction (CI) calculations in a similar way as in Ref. [44]. The experimental XAS and XMCD line shapes have been compared to those derived from theoretical calculations and the $\langle T_z \rangle / \langle S_z \rangle$ value corresponding to the best match has been used in the sum-rules analysis. To get an idea of the uncertainty introduced by the $\langle T_z \rangle$ term, the values of $\langle S_z \rangle$ have been also calculated assuming $\langle T_z \rangle = 0$. As shown in Table II, a 25% difference is obtained. However, the strong difference in the m_l/m_s ratio is kept. In a similar way, although CI calculations indicate that the $\langle T_z \rangle$ term is sensitive to band effects in iridates, the associated factor of uncertainty does not change our overall conclusions regarding the m_l/m_s ratio.

In addition, from the analysis of the XMCD spectra it can be concluded that neither a pure CEF-derived nor a pure j_{eff} electronic state can explain all the spectra. On the other hand, the diversity of spectra can be accounted for by considering the actual electronic band structure as the result of a delicate balance between CEF and SOC and structural degrees of freedom that may change from one oxide to another. Thus, the quenched orbital magnetic moment of Ca, Zn, and Mg perovskites, resembling a classical transition-metal oxide (TMO) case with wide CEF bands, can be tentatively accounted for in terms of bandwidth increase due to Ir-O bond shortening. The fact that a mixture of 78% of the lowest multiplet and 22% of the first-excited multiplet has to be included in the theoretical model in order to match the experimental profiles supports the idea that the states become mixed due to band effects in the Ir^{6+} compounds. On the other hand, the overall reduction at the $L_{3,2}$ edges for the Ir^{5+} oxides and the strong reduction of L_2 XMCD for Sr_2TiIrO_6 highlights the influence of the SOC in the definition of the $5d$ orbitals since in the strong SOC limit, with pure $j_{\text{eff}} = \frac{1}{2}$ and $\frac{3}{2}$ subbands, one would expect no XMCD for the Ir^{5+} samples and no L_2 XMCD for the Ir^{4+} samples. Besides, for a $j_{\text{eff}} = \frac{1}{2}$ state, one expects L_z parallel to S_z and L_z/S_z close to 1, which is what we observe for the compounds with M = Sc, In, and Ti.

As for the small differences between compounds with the same nominal electronic occupation, for instance between Sc and In compounds, these could be due to deviations from the nominal valence. However, the differences observed cannot be simply explained in terms of mixed valence Ir^{5+} and Ir^{6+} states. Alternatively (or additionally), they can be tentatively attributed to antisite disorder, slight differences in the Ir-O-Ir angle and/or IrO_6 deviations from O_h symmetry causing slight differences in the hybridization and the resulting electronic states. In this respect, CI calculations indicate that small band effects, exchange fields, and/or structural details have relatively large consequences in the spectral line shape of iridates.

Regardless of the details of the electronic structure, it is worth emphasizing that the new states in the $5d$ band have a magnetic moment which has both orbital and spin components. This is in stark contrast to the classical TMO case, where the hole in the t_{2g} levels could pick an orbital and choose its spin independently. This might be of great potential interest for spintronic applications.

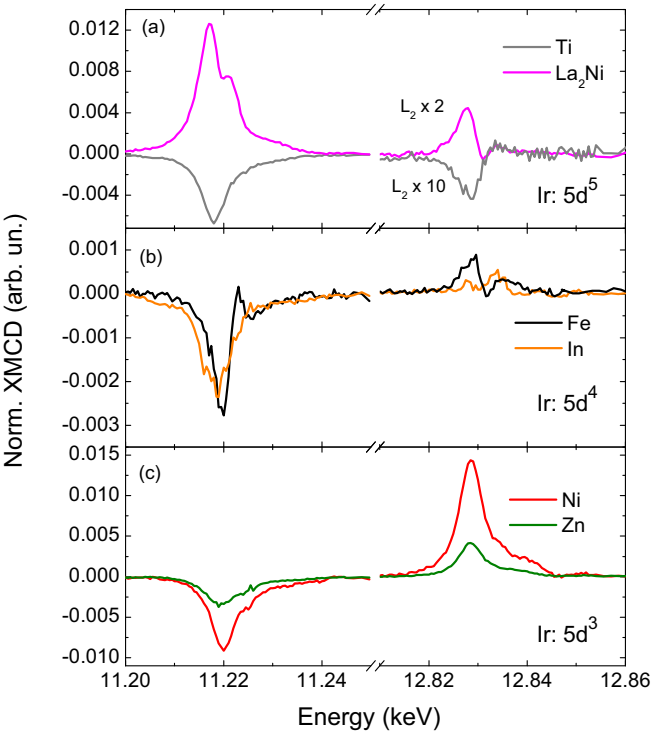

FIG. 9. (Color online) (a) Ir $L_{3,2}$-edge XMCD spectra of the Ir^{4+} oxides recorded at $T = 6$ K and $H = 3.5$ T. (b) Ir $L_{3,2}$-edge XMCD spectra of the Ir^{5+} oxides recorded at $T = 6$ K and $H = 3.5$ T. (c) Ir $L_{3,2}$-edge XMCD spectra of the Ir^{6+} oxides recorded at $T = 6$ K and $H = 3.5$ T.

XMCD spectra have also been recorded for several double perovskites with magnetic $3d$ atoms (see Fig. 9). The opposite sign of the XMCD spectra for La_2NiIrO_6 and Sr_2TiIrO_6 shows that the Ir net moment aligns antiparallel to the Ni net moment, which is is further verified by sum-rules analysis. The higher m_{tot} in La_2NiIrO_6, almost twice that of Sr_2TiIrO_6, and the richer line-shape profile (two well-resolved features can be distinguished at both edges) suggests that a significant magnetic moment is induced by interaction with the magnetic $3d$ ion. The holes in the Ni $3d$ band may give rise to changes in hybridization and electronic structure. However, the fact that both compounds show a similar value for the L_z/S_z ratio (its 20% difference is significantly smaller than the ~90% increase in m_{tot}) along with the AFM arrangement within the Ir sublattice, prevent us from directly associating the excess of magnetic moment to an induced contribution. The differences in the total ordered moment could be due to a different canting angle between the magnetic moments. In that case, further narrowing of the $5d$ bands due to larger tilting angles could also contribute to the modification of the XMCD profile.

Regarding the Ir^{5+} samples, Sr_2FeIrO_6 shows the same sign as Sr_2InIrO_6 at both edges. This indicates that the net magnetic moment of Ir orders parallel to the net Fe moment. The electronic change inferred from the richer L_3-edge profile of Sr_2FeIrO_6 is verified by sum rules indicating that L_z decreases to become twice smaller than S_z. The observed modifications may be related to an induced component due to Fe polarization effects. A structure-driven origin seems, in this compound, less likely: the Ir-O bond distance is only slightly smaller in the

case of M = Fe and the degree of distortion in the octahedral environment around Ir is very similar for the three compounds. The specific octahedra tilting $a^-a^-c^+$ for In and Sc ($P2_1/n$) and $a^0b^-b^-$ for Fe ($I2/m$) could explain differences in the calculated m_{tot} but not in the L_z/S_z ratio.

In Sr_2NiIrO_6, no signal reversal is observed. Therefore, the net moments of Ir and Ni order parallel. In addition, no difference other than a change in the intensity is observed in the XMCD profile of Sr_2NiIrO_6 relative to the other Ir^{6+} samples. Sum rules indicate a significant increase of both the total moment and the L_z/S_z ratio relative to compounds with no magnetic M and suggest a 3d-induced contribution. A relative increase of $\langle L_z \rangle$ associated with a Ni-induced polarization effect is supported by Ni XMCD data recorded in other oxides: a L/S ratio of 0.27 for $NiFe_2O_4$ [47] and 0.49 for La_2NiMnO_6 [48]. Calculations on $NiFe_2O_4$ give $L/S = 0.36$ for Ni and only 0.01 for Fe [49]. In addition, the presence of 3d holes in the of Sr_2NiIrO_6 may affect the hopping of electrons resulting in a more localized 5d state due to the large onsite Coulomb repulsion at Ni sites. On the other hand, according to diffraction data, Sr_2NiIrO_6 has $\sim$1% larger Ir-O band distances and so a structure-driven modification cannot be ruled out.

Our results show that the 3d-5d net coupling changes from sample to sample, illustrating the high complexity of competing antiferromagnetic interactions in 3d-5d double perovskites. In these compounds, the structural details are bound to strongly influence the strength and nature of magnetic ordering. Similar results highlighting the subtle links between structure and magnetism have been reported in Osmium, chemical element (Os) double perovskites [50]. The d occupancy, which also changes from one sample to another, is an additional factor determining the strength of the 3d-5d exchange and therefore the magnetic structure, especially the net magnetization in the Ir sublattice measured by XMCD in an applied field. Further information is necessary to fully understand how both structure and d occupancy determine the strength of the different competing superexchange pathways and the resulting magnetic structure.

In addition, the XMCD spectra in double perovskites with magnetic 3d atoms suggests the presence of an induced moment, as suggested for La_2CoIrO_6 [51]. However, the high sensitivity of the magnetic structure of iridates to structural details prevents us from directly obtaining the induced moment as the difference in m_{tot}(magnetic M) $-$ m_{tot}(no magnetic M).

IV. SUMMARY AND CONCLUSIONS

In summary, a series of Sr_2MIrO_6 and La_2NiIrO_6 double perovskites have been studied with element- and orbital- (Ir-5d) specific x-ray absorption spectroscopy measurements. The analysis of the $L_{2,3}$-edge XAS spectra indicates a strong spin-orbit coupling $\langle \mathbf{L} \cdot \mathbf{S} \rangle \sim 1.9$–$2.9$ in units of $\hbar^2$, in all the 5d TMOs samples and independently on the character of the magnetic moment. Moreover, the evolution of $\langle \mathbf{L} \cdot \mathbf{S} \rangle$ with the electronic occupation reflects the strong influence of the SOC on the electronic band structure. In addition, the orbital and spin contributions to the Ir magnetic moment have been disentangled by XMCD. We find that the Ir 5d magnetic moment shows different character depending on the oxidation state even when the total magnetic moment value is comparable for all the compounds. Thus, Ir carries an orbital contribution comparable to the spin contribution for Ir^{4+} and Ir^{5+} oxides, whereas the orbital contribution is quenched for Ca, Zn, and Mg samples. Our results also indicate that increased covalence with increasing valence quenches the orbital moment faster than the spin moment. The details of the actual electronic band structure, determined by a delicate balance between CEF, SOC, and structural degrees of freedom, seem to vary from one oxide to another within the Sr_2MIrO_6 series.

Including a magnetic 3d atom illustrates the complexity of the magnetic interactions in these oxides. We find that in Sr_2FeIrO_6 and Sr_2NiIrO_6, the net moment of Ir aligns parallel to the net magnetic moment of Fe and Ni, respectively. By contrast, it aligns antiparallel to Ni in La_2NiIrO_6. This points out the key role of structure and d-orbital occupancy in the magnetic structure of A_2MIrO_6 double perovskites. Moreover, our XMCD data suggest the presence of a 3d-induced contribution whose details would depend not only on the particular 3d atom, but also on the structural details such as bond lengths and angles.

ACKNOWLEDGMENTS

This work was partially supported by the Spanish MINECO Projects No. MAT2014-54425-R and No. MAT2013-41099-R and by the Comunidad de Madrid Project No. S2009PPQ-1551. M. A. Laguna-Marco acknowledges CSIC and European Social Fund for a JAE-Doc contract. Use of the Advanced Photon Source, an Office of Science User Facility operated for the U.S. Department of Energy (DOE) Office of Science by Argonne National Laboratory, was supported by the U.S. DOE under Contract No. DE-AC02-06CH11357. The authors are grateful to M. García-Hernández for the magnetic measurements and to J. Chaboy for fruitful discussions.

[1] J. G. Bednorz and K. A. Müller, Z. Phys. B: Condens. Matter **64**, 189 (1986).
[2] Y. Tokura and N. Nagaosa, Science **288**, 462 (2000).
[3] K.-I. Kobayashi, T. Kimura, H. Sawada, K. Terakura, and Y. Tokura, Nature (London) **395**, 677 (1998).
[4] R. Ramesh and N. Spaldin, Nat. Mater. **6**, 21 (2007).
[5] A. A. Aligia, P. Petrone, J. O. Sofo, and B. Alascio, Phys. Rev. B **64**, 092414 (2001).
[6] H. Kato, T. Okuda, Y. Okimoto, Y. Tomioka, K. Oikawa, T. Kamiyama, and Y. Tokura, Phys. Rev. B **65**, 144404 (2002).
[7] A. Poddar and S. Das, Physica B (Amsterdam) **344**, 325 (2004).
[8] J. B. Philipp, P. Majewski, L. Alff, A. Erb, R. Gross, T. Graf, M. S. Brandt, J. Simon, T. Walther, W. Mader *et al.*, Phys. Rev. B **68**, 144431 (2003).

[9] B. J. Kim, H. Jin, S. J. Moon, J.-Y. Kim, B.-G. Park, C. S. Leem, J. Yu, T. Noh, C. Kim, S.-J. Oh *et al.*, Phys. Rev. Lett. **101**, 076402 (2008).

[10] B. J. Kim, H. Ohsumi, T. Komesu, S. Sakai, T. Morita, H. Takagi, and T. Arima, Science **323**, 1329 (2009).

[11] D. A. Zocco, J. J. Hamlin, B. D. White, B. J. Kim, J. R. Jeffries, S. T. Weir, Y. K. Vohra, J. W. Allen, and M. B. Maple, J. Phys.: Condens. Matter **26**, 255603 (2014).

[12] G. Cao, X. N. Lin, S. Chikara, V. Durairaj, and E. Elhami, Phys. Rev. B **69**, 174418 (2004).

[13] G. Cao, V. Durairaj, S. Chikara, L. E. DeLong, S. Parkin, and P. Schlottmann, Phys. Rev. B **76**, 100402 (2007).

[14] Y. Okamoto, M. Nohara, H. Aruga-Katori, and H. Takagi, Phys. Rev. Lett. **99**, 137207 (2007).

[15] G. Jackeli and G. Khaliullin, Phys. Rev. Lett. **102**, 017205 (2009).

[16] A. Shitade, H. Katsura, J. Kuneš, X.-L. Qi, S.-C. Zhang, and N. Nagaosa, Phys. Rev. Lett. **102**, 256403 (2009).

[17] D. Pesin and L. Balents, Nat. Phys. **6**, 376 (2010).

[18] M. J. Lawler, H.-Y. Kee, Y. B. Kim, and A. Vishwanath, Phys. Rev. Lett. **100**, 227201 (2008).

[19] X. Wan, A. M. Turner, A. Vishwanath, and S. Y. Savrasov, Phys. Rev. B **83**, 205101 (2011).

[20] F. Wang and T. Senthil, Phys. Rev. Lett. **106**, 136402 (2011).

[21] T. K. Mandal, C. Felser, M. Greenblatt, and J. Kübler, Phys. Rev. B **78**, 134431 (2008).

[22] M. A. Laguna-Marco, G. Fabbris, N. M. Souza-Neto, S. Chikara, J. S. Schilling, G. Cao, and D. Haskel, Phys. Rev. B **90**, 014419 (2014).

[23] D. Haskel, G. Fabbris, M. Zhernenkov, P. P. Kong, C. Q. Jin, G. Cao, and M. van Veenendaal, Phys. Rev. Lett. **109**, 027204 (2012).

[24] S. J. Moon, H. Jin, K. Kim, W. S. Choi, Y. S. Lee, J. Yu, G. Cao, A. Sumi, H. Funakubo, C. Bernhard *et al.*, Phys. Rev. Lett. **101**, 226402 (2008).

[25] A. Lupascu, J. P. Clancy, H. Gretarsson, Z. Nie, J. Nichols, J. Terzic, G. Cao, S. S. A. Seo, Z. Islam, M. H. Upton *et al.*, Phys. Rev. Lett. **112**, 147201 (2014).

[26] O. B. Korneta, S. Chikara, S. Parkin, L. E. Delong, P. Schlottmann, and G. Cao, Phys. Rev. B **81**, 045101 (2010).

[27] D.-Y. Jung, G. Demazeau, and J.-H. Choy, J. Mater. Chem. **5**, 517 (1995).

[28] J. Rodriguez-Carvajal, Physica B (Amsterdam) **192**, 55 (1993).

[29] K. Hirano, K. Izumi, T. Ishikawa, S. Annaka, and S. Kikuta, Jpn. J. Appl. Phys. **30**, L407 (1991).

[30] J. C. Lang and G. Srajer, Rev. Sci. Instrum. **66**, 1540 (1995).

[31] M. Suzuki, N. Kawamura, M. Mizumaki, A. Urta, H. Maruyama, S. Goto, and T. Ishikawa, Jpn. J. Appl. Phys. **37**, L1488 (1998).

[32] P. Kayser, M. J. Martinez-Lope, J. A. Alonso, M. Retuerto, M. Croft, A. Ignatov, and M. T. Fernandez-Diaz, Inorg. Chem. **52**, 11013 (2013).

[33] P. Kayser, M. J. Martinez-Lope, J. A. Alonso, M. Retuerto, M. Croft, A. Ignatov, and M. T. Fernandez-Diaz, Eur. J. Inorg. Chem. **2014**, 178 (2014).

[34] P. Kayser, M. J. Martinez-Lope, J. A. Alonso, F. Mompeán, M. Retuerto, M. Croft, A. Ignatov, and M. T. Fernandez-Diaz (unpublished).

[35] J. Chaboy, J. Synchr. Rad. **16**, 533544 (2009).

[36] M. Tromp, J. Moulin, G. Reid, and J. Evans, AIP Conf. Proc. **882**, 669 (2007).

[37] P. Glatzel, G. Smolentsev, and G. Bunker, J. Phys.: Conf. Ser. **190**, 012046 (2009).

[38] N. Narayanan, D. Mikhailova, A. Senyshyn, D. M. Trots, R. Laskowski, P. Blaha, K. Schwarz, H. Fuess, and H. Ehrenberg, Phys. Rev. B **82**, 024403 (2010).

[39] Y. Jeon, B. Qi, F. Lu, and M. Croft, Phys. Rev. B **40**, 1538 (1989).

[40] V. V. Krishnamurthy, M. Suzuki, N. Kawamura, T. Ishikawa, and Y. Kohori, Hyperfine Interact. **136-137**, 361 (2001).

[41] G. Schütz, R. Wienke, W. Wilhelm, W. Wagner, P. Kienle, R. Zeller, and R. Frahm, Z. Phys. B: Condens. Matter **75**, 495 (1989).

[42] F. Wilhelm, P. Poulopoulos, H. Wende, A. Scherz, K. Baberschke, M. Angelakeris, N. K. Flevaris, and A. Rogalev, Phys. Rev. Lett. **87**, 207202 (2001).

[43] G. van der Laan and B. T. Thole, Phys. Rev. Lett. **60**, 1977 (1988).

[44] M. A. Laguna-Marco, D. Haskel, N. Souza-Neto, J. C. Lang, V. V. Krishnamurthy, S. Chikara, G. Cao, and M. van Veenendaal, Phys. Rev. Lett. **105**, 216407 (2010).

[45] B. T. Thole, P. Carra, F. Sette, and G. van der Laan, Phys. Rev. Lett. **68**, 1943 (1992).

[46] P. Carra, B. T. Thole, M. Altarelli, and X. Wang, Phys. Rev. Lett. **70**, 694 (1993).

[47] G. van der Laan, C. M. B. Henderson, R. A. D. Pattrick, S. S. Dhesi, P. F. Schofield, E. Dudzik, and D. J. Vaughan, Phys. Rev. B **59**, 4314 (1999).

[48] H. Guo, A. Gupta, M. Varela, S. Pennycook, and J. Zhang, Phys. Rev. B **79**, 172402 (2009).

[49] V. N. Antonov, B. N. Harmon, and A. N. Yaresko, Phys. Rev. B **67**, 024417 (2003).

[50] R. Morrow, J. W. Freeland, and P. M. Woodward, Inorg. Chem. **53**, 7983 (2014).

[51] A. Kolchinskaya, P. Komissinskiy, M. B. Yazdi, M. Vafaee, D. Mikhailova, N. Narayanan, H. Ehrenberg, F. Wilhelm, A. Rogalev, and L. Alff, Phys. Rev. B **85**, 224422 (2012).